OBSERVATION OF ORBITAL DEBRIS WITH SPACE-BASED SPACE SURVEILLANCE CONSTELLATIONS

Cristina Santana [(1)], Juan Carlos Dolado [(2)], Alfredo Antón [(3)]

[(1)] GMV Innovating Solutions, 17 Rue Hermès, Ramonville St. Agne
[(2)] CNES, 18 Avenue Edouard Belin, Toulouse
[(3)] GMV Innovating Solutions, Isaac Newton 11, Tres Cantos, 28760 Madrid

ABSTRACT

Since the first orbital launch back in 1957, the population of space debris in orbit around the Earth has steadily risen.

As the orbital debris population grows, the likelihood of catastrophic phenomena like the collision between two orbiting objects increases. In order to limit the proliferation of space debris in orbit, a great number of standards, guidelines and even laws have been put in place since the end of the 90's. In this scenario, a thorough and accurate bookkeeping of space objects is paramount. Space surveillance has thus become our most reliable ally to safeguard space missions from the threat of collisions.

The BAS^{3}E simulator *(Banc d´Analyse et de Simulation d'un Système de Surveillance de l'Espace)* is a CNES software tool, developed in collaboration with GMV. Using such space surveillance system simulator, this paper evaluates the feasibility to use on-board sensors for both Low Earth Orbit (LEO) and Geostationary Orbit (GEO) object surveillance. The main goal is to assess the ability of space-based space surveillance sensor (SBSS) constellations to detect and catalogue the space debris population on these both orbital regimes.

Index Terms— Space Based Sensors, Space Based Space Surveillance, Space Debris

1. INTRODUCTION

This paper presents the results of the study to evaluate the feasibility to use space-based sensors for both Low Earth Orbit and Geostationary Orbit object surveillance. In order to achieve this, simulations were conducted for various SBSS constellations for which their altitude and number of sensors were varied. The analysis of these simulations focused on the following points:

- Attitude constraints: angular velocity and angular acceleration required by sensors in order to detect, track and catalogue a given space object.
- Sensor optical characteristics: luminosity detectability threshold.
- Characterization of the space debris population which can be observed: duration of visibility periods, number of observations and number of observed objects during a given time period
- Orbit determination accuracy that can be attained when space objects are tracked by different space-based sensor configurations.

2. BAS^{3}E

The BAS^{3}E simulator is a CNES software tool, developed in collaboration with GMV. It is implemented in Java and makes use of a CNES orbital dynamics library named PATRIUS [1]. Some of its capabilities are: orbit determination of space objects, generation of optimum observation plans, collision forecast, anticipation to dangerous reentries, and detection of debris fragmentation. Furthermore, BAS^{3}E has the capability to simulate observations of space objects obtained by a given sensor network taking into account sensor visibility constraints. For each sensor, parameters such as orbit and attitude ephemerides, quality, precision, and usage cost shall be defined.

BAS^{3}E handles both ground-based observations (on-ground telescopes and radars) and space-based space surveillance sensors. The latter are defined as "orbiting" sensor sites. The orbit of these mobile sites can be determined either by a set of orbital parameters together with a propagation model or by an ephemeris file.

3. GENERAL ASSUMPTIONS AND MODELS

3.1. Space Debris population

Low Earth Orbit and Geostationary Orbit space debris population were considered for the study. The LEO population was taken from ESA's debris catalogue MASTER-2009 and consisted of 20811 objects, whereas the GEO population was computed making use of the MEDEE software tool from CNES [2] and consisted of 536 objects.

The orbits of all objects belonging to both populations were propagated for a period of 10 days making use of the propagation models defined in Table 1.

	LEO	GEO
Third body perturbations	Sun and Moon gravity forces	Sun and Moon gravity forces
Atmospheric drag	Numerical MSISE2000 atmosphere model for constant solar activity (solar flux: 175; geomagnetic idx: 15)	Not considered
Solar Radiation Pressure	Not considered	Considered
Earth Potential	12x12	12x12
Integrator	Runge-Kutta Dormand Prince method, min step size of 10s, max step size of 120 s.	Runge-Kutta Dormand Prince method, min step size of 10s, max step size of 120 s.
Earth Model	WGS84	WGS84

Table 1: Propagation models for simulation

4. SBSS SENSOR CONSTELLATIONS

Simulations were conducted for different constellations of spacecraft evenly spaced (in terms of mean anomaly) in quasi-circular, Sun-synchronous dawn-dusk orbits, for which the constellation altitudes and number of spacecraft were varied. In addition, spacecraft were considered to be equipped with one sensor, dedicated to space surveillance activities.

The studied constellations are defined in Table 2.

Altitude [km]	Number of spacecraft
500	5, 10, 20
750	2, 4, 8
1000	2, 4, 8

Table 2: SBSS constellation configurations

5. VISIBILITY CONSTRAINTS

The time periods when objects could be observed were computed. We refer to them as "visibility opportunities" and correspond to the time periods when all of the below mentioned observation constraints were fulfilled.

For simplicity reasons, we assumed that spacecraft followed an attitude profile which ensured the pointing of the on-board sensor towards the object. This assumption permitted the study of the attitude constraints required by each satellite in order to detect, track and catalogue a given space object.

The following visibility constraints were considered:

- **South Atlantic Anomaly (SSA):** During the passage through this region of intense radiation, sensors are exposed to a high energetic particle flux which affects its performance. Therefore it has been considered that the sensor is unable to observe objects during these periods. For simplicity, this region has been modelled as a rectangular area: longitude: [-90, -40] deg; latitude; [-50, 0] deg.
- **Angle between sensor boresight and Sun direction:** The proximity of the Sun to the sensor field-of-view (FOV) results in the sensor blinding, thus in the incapacity of the sensor to observe objects. The imposed minimum angle between the sensor boresight and Sun direction was 90 deg.
- **Angle between sensor boresight and Moon direction:** The proximity of the Moon to the sensor FOV results in the sensor blinding, thus in the incapacity of the sensor to observe objects. The imposed minimum angle between the sensor boresight and Moon direction was 20 deg.
- **Angle between sensor boresight and Earth direction:** Objects which are hidden by the Earth aren't observable by the sensor. In addition, the proximity of the Earth to the sensor FOV results in the sensor blinding, thus in the incapacity of the sensors to observe objects. The imposed minimum angle between the sensor boresight and Earth direction was 20 deg.
- **Angle between sensor boresight and Galactic plane:** The galactic plane is the plane in which the majority of the disk-shaped galaxy's mass lies. It is a strong source of light, thus the difficulty to discern objects which are close to this area. The imposed minimum angle between the sensor boresight and the Galactic plane was 30 deg.

5. COMPUTATION OF STATISTICS

In order to evaluate the attitude constraints, sensor optical characteristics and percentage of observable space debris population, a characterization of the visibility periods was conducted based on the following statistics:

- Maximum angular velocity of sensors
- Maximum angular acceleration of sensors
- Maximum/Minimum solar phase angle
- Maximum/Minimum luminosity of observed objects
- Mean number of observed objects per day
- Mean number of visibility opportunities per day
- Duration of visibility opportunities

6. OBSERVATIONS

Observations were simulated for the periods of visibility. These were composed of three observation components: azimuth, elevation and luminosity. Table 3 displays the bias and noise considered for each of the above-mentioned observation components.

	Bias	Noise (sigma)
Azimuth	0.0 [deg]	0.001 [deg]
Elevation	0.0 [deg]	0.001 [deg]
Luminosity	0.0	0.0

Table 3: Observation components

Furthermore, computed observations were filtered according to the values of their luminosity component in order to simulate diverse sensor qualities (high quality sensors would be able to visualize less luminous objects than low quality sensors) and moreover, assess the impact of sensor qualities on the attained orbit determination accuracy. The considered luminosity thresholds were 12, 14 and 16 Mv.

6. ORBIT DETERMINATION

All in all, 27 orbit determinations scenarios were performed per space debris population to evaluate the orbit determination accuracy that could be attained when tracking space objects by different SBSS sensor constellations. The considered configurations are summarized in Table 4.

Altitude [km]	Luminosity thresholds (Mv)		
	12	**14**	**16**
500	Nº sensors: 5, 10, 20	Nº sensors: 5, 10, 20	Nº sensors: 5, 10, 20
750	Nº sensors: 2, 4, 8	Nº sensors: 2, 4, 8	Nº sensors: 2, 4, 8
1000	Nº sensors: 2, 4, 8	Nº sensors: 2, 4, 8	Nº sensors: 2, 4, 8

Table 4: Combination of performed orbit determinations

The only introduced dynamic mismodelling was in the degree and order of the Earth gravity potential: 12x12 was used to propagate the "real world" orbit, whereas just 8x8 was used for the reconstruction model. Table 5 and table 6 present the configuration used for the orbit determinations.

	LEO	GEO
Third body perturbations	Sun and Moon gravity forces	Sun and Moon gravity forces
Atmospheric drag	Numerical MSISE2000 atmosphere model for constant solar activity (solar flux: 175; geomagnetic idx: 15)	Not considered
Solar Radiation Pressure	Not considered	Considered
Earth Potential	8x8	8x8
Integrator	Runge-Kutta Dormand Prince method, min step size of 10s, max step size of 120 s.	Runge-Kutta Dormand Prince method, min step size of 10s, max step size of 120 s.
Earth Model	WGS84	WGS84

Table 5: Propagation models for orbit determinations

	LEO	GEO
Statevector estimation	Yes	Yes
Estimated parameters	Atmospheric drag multiplicative factor	None
Considered observations	Azimuth, elevation	Azimuth, elevation
Estimation method	Least-squares	Least-squares
Convergence criteria	Maximum position and velocity corrections of 0.1 [m] and 0.001 [m/s] respectively. Maximum WRMS correction of 1e-3.	Maximum position and velocity corrections of 0.1 [m] and 0.001 [m/s] respectively. Maximum WRMS correction of 1e-3.
Max number of iterations	20	20

Table 6: Estimation parameters

7. OVERVIEW OF BAS^{3}E EXECUTION

BAS^{3}E is composed of stages which may be executed sequentially in order to concatenate their inputs and outputs. Each of these stages realizes a certain type of computation. The concatenation of stages may be flexibly arranged by the user in order to define different case study scenarios. The stages executed for this particular study are briefly explained hereafter and their sequence graphically displayed in Figure 1.

- ***PopulateSensorDb:*** Generates an SQL database with the configured sensors.
- ***ImportObjectDb:*** Generates an SQL database with the input object population.
- ***PropagateObjectEphemeris:*** Propagates the orbits of the object population.
- ***VisibilityOpportunities:*** Takes into account the visibility constraints defined for each sensor to compute the periods of visibility of them for each of the considered objects. These are stored in binary files.
- ***VisibilityStatistics:*** Computes the defined statistics (i.e. maximum angular acceleration, maximum angular velocity, maximum solar phase angle … etc.) per visibility period.
- ***VisibilityStatisticsFiles:*** Dumps the binary files containing the visibility statistics to an ASCII file for plotting.
- ***SensorLoad:*** Computes the number of simultaneously tracked objects per sensor.
- ***SensorObservations:*** Computes the defined sensor observations during the visibility periods. These are stored in binary files.

- ***FilterObservations:*** Filters the computed observations according to the values of their luminosity observation component.
- ***OrbitDetermination:*** Performs the orbit determinations and updates the object database with the computed statevector.
- ***ComputeCovariance:*** Generates ASCII files with the computed covariance.

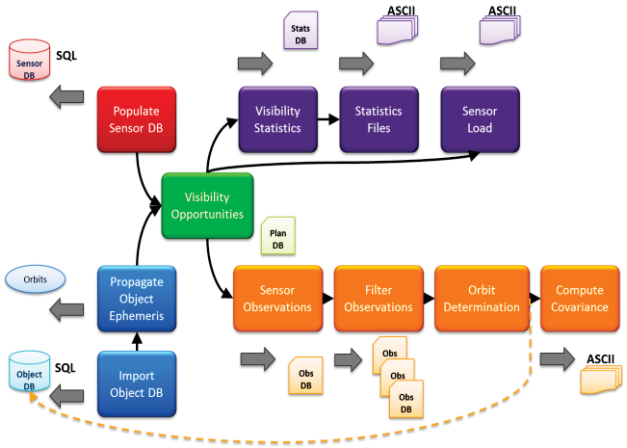

Figure 1: Overview in executed stages with BAS^{3}E

8. SURVEILLANCE OF OBJECTS IN LEO

An analysis of the surveillance of objects in LEO was performed. The most remarkable results are presented hereafter.

8.1. Visible space debris population

The visible space debris population in LEO was studied for all of the considered SBSS sensor constellations. A significantly disperse distribution of the visibility opportunities per day was observed which reveals the diversity of the considered LEO population in terms of eccentricity and semi-major axis. In addition a drop in the percentage of the visible population was appreciated with an increase of the constellation altitude (see Table 7). The LEO debris population has perigee altitudes within 100 km and 2000 km, thus, for constellations at higher altitudes the number of objects that are lower than the constellation altitude is larger. Consequently, due to the presence of the Earth, these objects are not observed.

Furthermore, only a marginal increase in the percentage of the visible population was appreciated with an increase in the number of sensors. Sensors belonging to the same constellation are in the same orbit, therefore, after a certain time, constellations at the same altitude would have achieved to track the same percentage of debris population.

On the other hand, the number of sensors results in an increase in the number of visibility opportunities per day. That is to say, the larger the number of sensors a constellation has, the higher the chances of observing an object. However, it is worth mentioning once more that these results do not take into account the limitation of sensors to track a maximum of one object at a time. Results represent the mean number of visibility opportunities per day that would be attained when attempting to observe a given object. This is in line with the fact that for this study sensors are assumed to operate in tracking mode and not in surveillance mode.

Moreover, an increase in the number of visibility opportunities per day was observed due to a decrease in altitude. This effect is intrinsically related to the percentage of debris population which is visible by constellations at such altitude.

By way of summation, and in simplistic terms, the altitude of the SBSS sensor constellations delimits the percentage of visible population whereas the number of sensors making up of the constellations establishes the number of visibility opportunities per day (frequency with which objects are observed).

Altitude [km]	**Number of sensors**		
	5	**10**	**20**
500	87.03%	87.05%	87.05%
	2	**4**	**8**
750	83.39%	83.66%	83.79%
1000	57.86%	58.14%	58.19%

Table 7: Percentage of visible population for surveillance of objects in LEO

Figure 2 displays the mean visibility opportunities per day for the constellation in a 500 km altitude orbit and 5 sensors. The plots obtained for the rest of configurations were very similar except for the aforementioned differences. In this case, for 50% of the population the mean visibility opportunities per day are around 10. This value increased by a multiplicative factor of 2 and 3for 10 and 20 sensors respectively. For the constellations in a 750 km and 1000 km altitude orbits, this number evolved in the same manner, except that for the minimum number of sensors the mean visibility opportunities per day for 50% of the population are around 5.

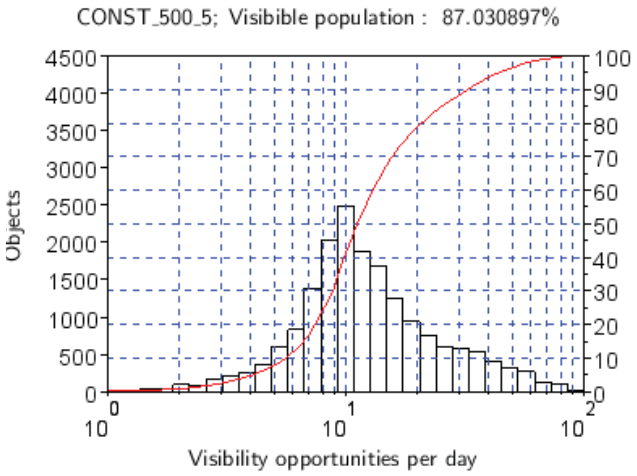

Figure 2: Mean visibility opportunities per day for surveillance of objects in LEO with a constellation in a 500[km] altitude orbit and 5 sensors

The following sections present the most remarkable results for the characterization of the "visibility opportunity" periods. Note that these are based on the space debris population which is visible for each constellation.

8.2. Visibility period durations

The most remarkable differences between the statistics computed for the various constellations were observed for the duration of the visibility periods. These results are summarized in Table 8. It can be observed that the duration of the visibility periods increased for increasing altitudes but remained unaltered for increasing number of sensors.

Altitude [km]	**Number of sensors**		
	5	**10**	**20**
500	Percentile 50%: 199 s	Percentile 50%: 199 s	Percentile 50%: 199 s
	2	**4**	**8**
750	Percentile 50%: 245 s	Percentile 50%: 245 s	Percentile 50%: 245 s
1000	Percentile 50%: 321 s	Percentile 50%: 321 s	Percentile 50%: 321 s

Table 8: Mean duration of visibility periods [s]; (surveillance of LEO population)

8.3. Attitude constraints

Figure 3 displays angular velocity against angular acceleration values. It shows an increase in the angular velocity with increasing angular acceleration as well as a maximum angular acceleration threshold value for a given angular velocity. Values for percentile 50% were around 5.0e-1 deg/s and angular acceleration for percentile 50% were around 3.0e-4 deg/s^2.

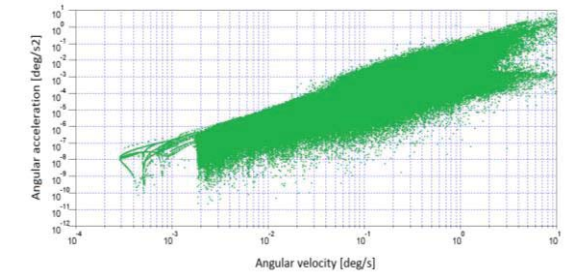

Figure 3: Relation between angular velocity and acceleration for surveillance of objects in LEO

Moreover, the influence of eccentricity and semi-major axis of the space object orbits on the mean maximum angular acceleration, mean angular velocity and duration of visibility opportunities was analyzed. This analysis reveals an increase in both angular velocity and acceleration with a decrease in eccentricity and semi-major axis unlike the duration of the visibility opportunities. The most likely explanation is that the visibility opportunities for eccentric orbits would occur more frequently closer to their apogee where objects speed is slower.

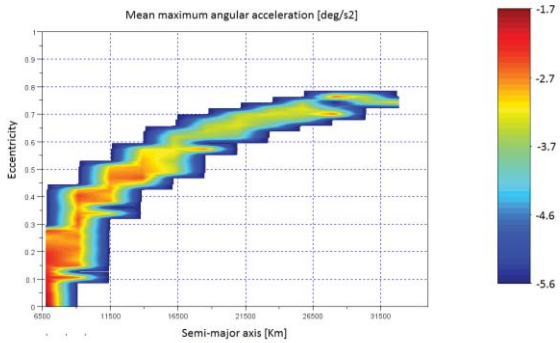

Figure 4: Mean maximum angular acceleration as a function of eccentricity and semi-major axis (The color legend is in logarithmic scale)

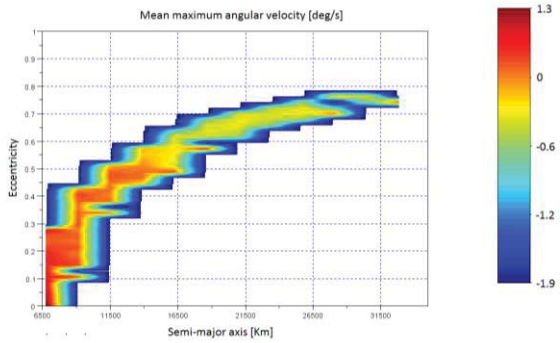

Figure 5: Mean maximum angular velocity as a function of eccentricity and semi-major axis (The color code legend is in logarithmic scale)

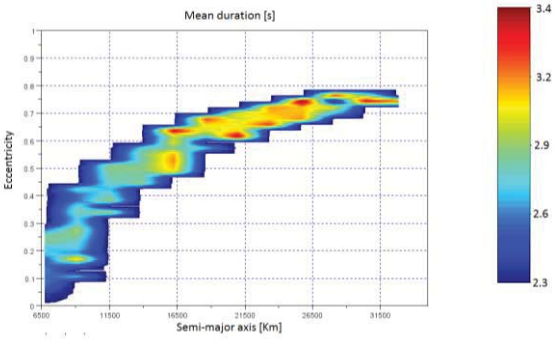

Figure 6: Mean duration as a function of eccentricity and semi-major axis (The color code legend is in logarithmic scale)

8.4. Magnitude

The relation between the object magnitude (expressed with respect to Vega) and both solar phase angle and object diameter was studied. A clear decrease in the observed object magnitude is appreciated with an increase of the object diameter. However, the solar phase angle values do not seem to have a remarkable impact on the magnitude. This unexpected result led us to conclude that other parameters at play with influence over the magnitude (i.e. distance between sensor and object), were eclipsing the effect of the solar phase angle.

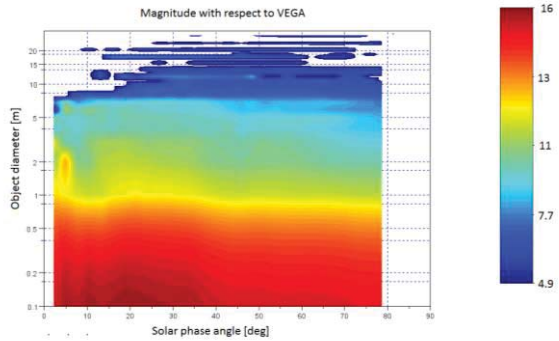

Figure 7: Object magnitude with respect to VEGA as a function of the solar phase angle and object diameter

In order to reaffirm this hypothesis, the evolution during random "visibility periods" of the involved parameters (solar phase angle, magnitude and distance between sensor and object) for a given sensor and given object was computed. Note that an increase in the solar phase angle contributes to an increase in magnitude; and an increase in the distance between sensor and object contributes to an increase in magnitude.

For the first case (Figure 8), both solar phase angle and distance between sensor and object decreased with time; and so behaved the magnitude. Nevertheless, for the second case (Figure 9), the solar phase angle decreased with time whereas the distance between sensor and object increased. In this particular case, the magnitude increased with time following the trend of the distance between sensor and object instead of the trend of the solar phase angle.

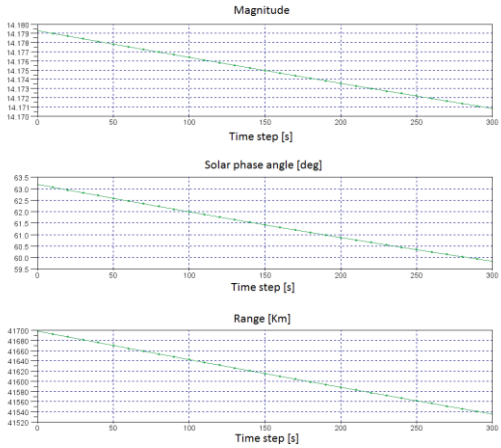

Figure 8: Evolution of solar phase angle and range during a "visibility opportunity" where magnitude follows the trend of the solar phase angle

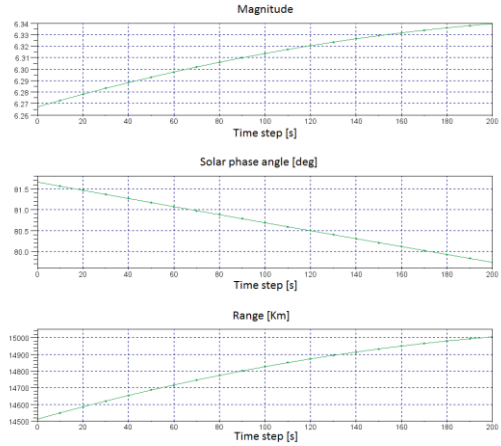

Figure 9: Evolution of solar phase angle and range during a "visibility opportunity" where magnitude follows the trend of the range

8.5. Orbit determination accuracy

Orbit determinations were conducted for each one of the considered scenarios. These were performed in a single batch for a time interval of 10 days. Furthermore all of the elevation and azimuth observations made during this period were taken into account. The values of orbit covariance, atmospheric drag coefficient and atmospheric drag covariance were computed for the end of the orbit restitution arc.

An improvement in the orbit determination accuracy could be observed with an increase in number of sensors as well as with a decrease in orbit altitude. As previously observed in this paper, both of these parameters result in an increase in visibility opportunities per day and consequently in the number of available observations.

Tables 9 and 10 summarize the percentage of objects for which the atmospheric drag coefficient was estimated with an error greater than 5 percent. This percentage decreases with an increase in both magnitude threshold and number of sensors as they result in an increase in number of observations. Although this trend can be observed for both eccentric and non-eccentric orbits, it is much more remarkable for the case of eccentric orbits. Furthermore, it is also for the case of eccentric orbits for which this percentage increases with an increase in the constellations altitude. As previously mentioned, constellations at higher altitude are able to observe a smaller percentage of the debris population. This is mainly due to the inability to observe objects which are below the constellations altitude. Therefore, constellations at higher altitudes do not observe objects at lower altitudes where the effect of the atmospheric drag is most significant.

Altitude [km]	Nº of sensors	Magnitude		
		12	14	16
500	5	22.2%	20.9%	16.5%
	10	19.7%	18.4%	14.4%
	20	18.8%	16.5%	14.3%
750	2	22.1%	20.9%	17.5%
	4	22.2%	21.0%	16.6%
	8	19.4%	18.7%	14.3%
1000	2	21.7%	22.4%	18.4%
	4	21.5%	20.7%	16.3%
	8	21.0%	18.3%	14.6%

Table 9: Percentage of objects in non-eccentric orbits (ecc<=0.1) for which their atmospheric drag coefficient was estimated with an error greater than 5 percent

Altitude [km]	Nº of sensors	Magnitude		
		12	14	16
500	5	22.0%	19.8%	10.5%
	10	17.0%	15.1%	7.9%
	20	12.5%	10.7%	6.7%
750	2	35.8%	31.3%	19.3%
	4	25.5%	23.0%	12.6%
	8	17.6%	15.5%	8.1%
1000	2	51.8%	44.4%	31.0%
	4	40.2%	33.3%	20.7%
	8	25.8%	20.9%	12.9%

Table 10: Percentage of objects in eccentric orbits (ecc>0.1) for which their air drag coefficient was estimated with an error greater than 5 percent

Figure 10 displays the position covariance of the along-track component for the 500 km altitude constellations and for the various number of sensors considered. A clear decrease in the covariance can be observed for increasing number of sensors. For the rest of the considered altitudes and magnitude thresholds similar plots were obtained. Just a slight decrease in the covariance is observed for decreasing altitudes and increasing magnitude thresholds. It can be appreciated that covariance is in the order of tens of meters for 50% of the observed objects. (Radial and cross-track components behave similarly. For 50% of the observed objects the radial position covariance is in the order of meters whereas the cross-track position covariance is around 20 m)

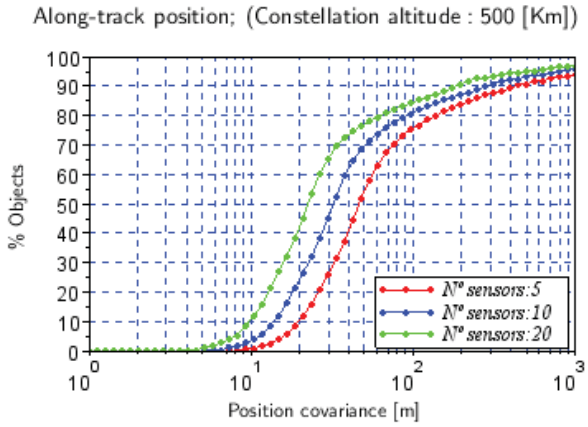

Figure 10: Covariance of along-track component for surveillance of LEO population with constellations in 500[km] altitude and magnitude threshold of 12

9. SURVEILLANCE OF OBJECTS IN GEO

An analysis of the surveillance of objects in GEO was performed similar to the one performed for the surveillance of objects in LEO. The most remarkable results are presented hereafter.

9.1. Visible space debris population

Contrary to what has been observed for the LEO population, the variation in the percentage of the visible population is marginal (maximum difference of 2%) between all of the considered configurations. Furthermore, the distribution of the visibility opportunities per day is not as dispersed as for the LEO population with average values around 10 to 25.

It is also worth mentioning what at first could seem inconsistent: there is a drop in the number of visibility opportunities per day for the configurations with maximum number of sensors. Visibility opportunities per day for a given object are computed as the sum of all the visibility opportunities of such object for all the sensors from a considered constellation. Nevertheless, in the event of

overlap of visibility opportunities of various sensors, these are counted as a single visibility opportunity. Therefore, the number of visibility opportunities increases with an increase in the number of sensors in a constellation until such increase leads to objects being observed simultaneously by various sensors from the same constellation.

Altitude [km]	Number of sensors		
	5	**10**	**20**
500	97.20%	97.20%	97.20%
	2	**4**	**8**
750	99.44%	99.44%	99.44%
1000	98.32%	98.32%	98.32%

Table 11: Percentage of visible population for surveillance of objects in GEO

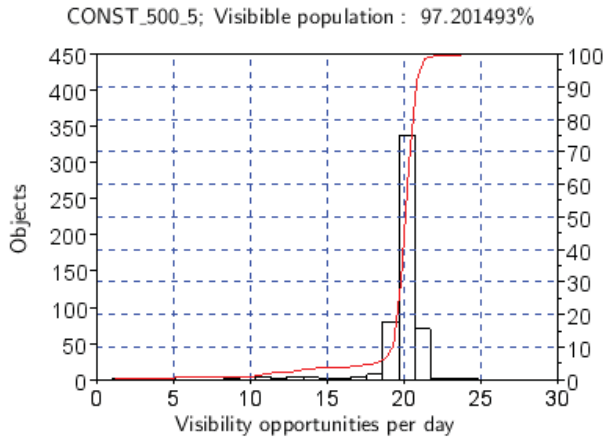

Figure 11: Mean visibility opportunities per day for surveillance of objects in GEO with a constellation in a 500[km] altitude orbit and 5 sensors

9.2. Visibility period durations

Table 12 summarizes the results regarding the duration of the visibility periods for the surveillance of objects in GEO. The same trend is observed as for the LEO case, besides considerable longer durations.

Altitude [km]	Number of sensors		
	5	**10**	**20**
500	Percentile 50%: 513 s	Percentile 50%: 513 s	Percentile 50%: 513 s
	2	**4**	**8**
750	Percentile 50%: 736 s	Percentile 50%: 736 s	Percentile 50%: 736 s
1000	Percentile 50%: 926 s	Percentile 50%: 926 s	Percentile 50%: 926 s

Table 12: Mean duration of visibility periods [s]; (surveillance of GEO population)

9.3. Attitude constraints

The relation between angular velocity and angular acceleration was similar to the LEO case with the only exception of the range of values of both variables. Angular velocity values for percentile 50% were around 4.0e-3 deg/s and angular acceleration for percentile 50% were around 3.0.e-7 deg/s^2. These values were much smaller than those observed for the LEO case.

9.4. Magnitude

The relation between the object magnitude (expressed with respect to Vega) and both solar phase angle and object diameter was identical to the one observed for the LEO case (cf. Figure 7).

9.5. Orbit determination accuracy

In the same manner as for the LEO case, orbit determinations were performed for the GEO case. Figure 12 displays the covariance for the along-track component. Similar to the LEO case, a decrease in covariance can be observed for increasing number of sensors. Also, for the rest of the considered altitudes and magnitude thresholds a slight decrease in the covariance was observed for decreasing altitudes and increasing magnitude thresholds. Furthermore, it can be appreciated that for 50% of the objects observed covariance is around 30 m. This represents a better accuracy than for the LEO case. (Radial and cross-track components behave similarly. For 50% of the observed objects both radial position covariance and cross-track position covariance are around 15 m)

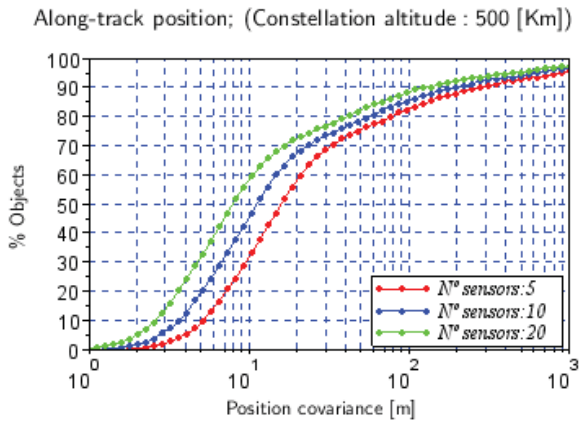

Figure 12: Covariance of along-track component for surveillance of GEO population with constellations in 500[km] altitude and magnitude threshold of 12

10. CONCLUSIONS

The assessment of the impact of the altitude and number of sensors of the SBSS constellations concludes as follows. The percentage of visible population is mainly delimited by the altitude of the SBSS sensor constellations for the surveillance of the LEO population. This percentage decreases with increasing altitudes. Meanwhile, for the surveillance of the GEO population, the altitude of the SBSS constellations has no impact on the percentage of visible population.

On the other hand, the number of sensors has an impact on the number of visibility opportunities per day (number of visibility opportunities per day increase with an increase in number of sensors).

Regarding the computed statistics, it was observed that these are more restrictive for the surveillance of the LEO population than for the GEO population. For the surveillance of the LEO population the duration of the visibility opportunities is shorter and moreover, the required angular velocity and acceleration are higher.

Concerning the percentage of visible population, in order to observe the largest percentage of the LEO population the SBSS sensor constellation in a 1000 km altitude orbit should be discarded. (58% of visible population for 1000 km versus 87% and 83% for 500 km and 750 km respectively). However for the GEO case results do not reveal an optimum SBSS sensor constellation.

Furthermore, with regards to the attitude constraints, no optimum SBSS sensor constellation stands out for the surveillance of both LEO and GEO populations.

Finally, in relation to the attained orbit determination accuracy, SBSS sensor constellations in 500 km orbits present the best accuracy which also improves with an increase in number of sensors and magnitude threshold. This was the case for the surveillance of both LEO and GEO populations.

11. REFERENCES

[1] Denis, C. and Tanguy, Y. "The SIRIUS Flight Dynamics Library for the next 25 years". *Proceedings of the 5th International Conference on Astrodynamics Tools and Techniques (ICATT)*

[2] Reference J.C. Dolado-Perez, R. Di-Costanzo, B. Revelin, Introducing MEDEE – "A New orbital debris evolutionary model", *Proceedings of the Sixth European Conference on Space Debris*, Darmstadt, Germany, 22–25 April, 2013, European Space Agency Publication (2013).